Computational exploration of the six-dimensional vibration–rotation–tunneling dynamics of $(NH_3)_2$

J. W. I. van Bladel, A. van der Avoird, and P. E. S. Wormer
Institute of Theoretical Chemistry, University of Nijmegen, Toernooiveld, 6525 ED Nijmegen, The Netherlands

R. J. Saykally[a)]
Department of Chemistry, University of California, Berkeley, California 94720

(Received 25 March 1992; accepted 27 April 1992)

In order to address the well-known problem that the nearly cyclic structure of $(NH_3)_2$ deduced from microwave spectra differs greatly from the hydrogen-bonded equilibrium structure obtained from *ab initio* calculations, we have calculated the vibration–rotation–tunneling (VRT) states of this complex, and explicitly studied the effects of vibrational averaging. The potential used is a spherical expansion of a site–site potential which was extracted from *ab initio* data. The six-dimensional VRT wave functions for all the lowest states with $J=0$ and $J=1$ were expanded in products of radial (van der Waals stretch) functions and free-rotor states for the internal and overall rotations, which were first adapted to the complete nuclear permutation inversion group G_{36}. Although the (expanded) potential is too approximate to expect quantitative agreement with the observed microwave and far-infrared spectra, we do find several interesting features: The ^{14}N quadrupole splittings and the dipole moment of the complex, which are indicative of the orientational distributions of the NH_3 monomers, are substantially affected by vibrational averaging. The interchange tunneling of the two monomers is not quenched. In the *ortho–ortho* and *para–para* states, of A and E symmetry, this tunneling manifests itself in a very different manner than in the *ortho–para* states of G symmetry. In contrast with the interpretation of Nelson *et al.* [J. Chem. Phys. **87**, 6364 (1987)], we believe that the G_α and G_β states observed by these authors correspond to a single VRT state which is split by (hindered) NH_3 monomer inversion.

I. INTRODUCTION

Hydrogen bonding plays an important role in many molecular systems of chemical and biological importance. The study of hydrogen-bonded van der Waals complexes can provide much insight into the nature of this phenomenon. Both $(HF)_2$ and $(H_2O)_2$ have been studied[1] extensively by both theoreticians and experimentalists. Calculations have predicted that these complexes possess a hydrogen-bonded structure and experiments confirm this finding. Another prototypical example of a hydrogen-bonded system would be $(NH_3)_2$, in which one NH_3 monomer acts as a proton donor and the other one as a proton acceptor. This picture is supported by several *ab initio* calculations.[1] However, microwave experiments[2,3] have been interpreted as showing that it is not valid. The structure deduced from the microwave data is a nearly cyclic one, in which both monomers act simultaneously as proton donors and acceptors. The only *ab initio* calculation which predicts such a structure was performed by Sagarik, Ahlrichs, and Brode.[4] We have found, however, that the minimum in their model potential, which they fitted to the *ab initio* data, actually occurs also at a structure with a nearly linear hydrogen bond.

Vibrational averaging has been proposed[5] as an explanation for the discrepancy between theory and experiment. The calculated potential surface is very flat in some directions,[4,5] such that the vibrationally averaged structure could indeed deviate considerably from the equilibrium structure found in *ab initio* calculations. Microwave experiments by Nelson *et al.*[3] with isotopomers of $(NH_3)_2$ seem to disprove this possibility, however. Because of all these features, the NH_3 dimer takes a special place among the hydrogen-bonded van der Waals complexes. In the review paper of Buckingham, Fowler, and Hutson[1] a special section is devoted to "the strange case of the ammonia dimer." Furthermore, it should be noted that the microwave experiments[2,3] probe only one of the three possible nuclear-spin species (see Sec. IV), *viz.* that which supports purely rotational transitions. It is quite possible that the structures of the other species are different from this one.

In the present paper we describe full six-dimensional dynamics calculations of the vibration–rotation–tunneling (VRT) levels of the NH_3 dimer, using the site–site potential of Sagarik, Ahlrichs, and Brode.[4] We investigate whether the vibrationally averaged structures obtained for each nuclear-spin species indeed deviate from the *ab initio* equilibrium structure, and whether this reconciles the *ab initio* calculations with the experiments. An energy-level scheme is presented, and the nature of some van der Waals states and some observed far-infrared transitions are discussed. Note that the calculations must be considered as semiquantitative. They are mainly intended to give a qualitative understanding of the spectrum. The calculation of a

[a)]Visiting professor at the Institute of Theoretical Chemistry, Research Institute of Materials, University of Nijmegen (July 1991).

 0021-9606/92/194750-14$006.00 © 1992 American Institute of Physics

Downloaded 13 Jun 2006 to 128.32.220.140. Redistribution subject to AIP license or copyright, see http://jcp.aip.org/jcp/copyright.jsp

full *ab initio* potential surface and the subsequent calculation of fully converged rovibrational states are still beyond the scope of present-day computers.

II. THE INTERMOLECULAR POTENTIAL

In the coordinate system used, the vector **R** connects the centers of mass of the NH_3 monomers. This vector has length R and polar angles β and α relative to a space-fixed frame. The dimer frame is defined as the frame in which the vector **R** lies along the z axis. This (embedded) frame is related to the space-fixed frame by rotations over the angles α and β. Further, we define two monomer frames which are principal axes frames of NH_3 with their origins at the centers of mass of the NH_3 monomers. Within such a principal axes frame, the nitrogen nucleus is located on the positive z axis and one of the hydrogen nuclei lies in the xz plane with positive x. The monomer frames are related to the dimer frame by the Euler angles γ_A, ϑ_A, and φ_A for monomer A and γ_B, ϑ_B, and φ_B for monomer B, as specified for Ar–NH_3 in Ref. 6. The C_3 axes of NH_3 have polar angles ϑ_A, γ_A, and ϑ_B, γ_B with respect to the dimer frame. The angles φ_A and φ_B describe rotations around the C_3 axes. The dihedral angle γ is defined as the difference $\gamma_B - \gamma_A$. From the microwave and infrared experiments of Fraser *et al.*[7] Nelson, Fraser, and Klemperer[2] conclude that the umbrella inversion motions of the NH_3 monomers are completely quenched in $(NH_3)_2$. Therefore, we have neglected the inversion tunneling in these calculations.

Sagarik, Ahlrichs, and Brode[4] have obtained their intermolecular potential by performing *ab initio* calculations for five different orientational geometries of the dimer, varying only the three geometrical parameters that correspond to our coordinates R, ϑ_A, and ϑ_B. Note that they choose the origins of the monomers at the nitrogen nuclei rather than at the NH_3 centers of mass. In total, 75 dimer configurations were computed. The results were fitted to a site–site potential in order to get a full potential-energy surface. We are aware that this potential is rather crude, but it is the only *full* surface available at present. Sagarik, Ahlrichs, and Brode have used their site–site potential to perform molecular-dynamics calculations on liquid NH_3. In this paper we use their potential to investigate the rovibrational and tunneling van der Waals levels of $(NH_3)_2$. The analytical form of the site–site potential is[4]

$$V=\sum_{i\in A}\sum_{j\in B}\left[A_{ij}\exp(-B_{ij}r_{ij})+q_iq_jr_{ij}^{-1}-C_{ij}F_{ij}(r_{ij})r_{ij}^{-6}\right] \tag{1a}$$

with

$$F_{ij}(r_{ij})=\begin{cases}\exp[-(1.28r_{ij}^0/r_{ij}-1)^2] & \text{for } r_{ij}<1.28r_{ij}^0\\ 1 & \text{for } r_{ij}\geqslant 1.28r_{ij}^0\end{cases}, \tag{1b}$$

where i and j label the sites in the monomers A and B and r_{ij} denotes the distance between two sites. The force centers on each monomer are the hydrogen atoms and a site 0.08 Å below the nitrogen atom towards the hydrogen atoms. The parameters appearing in Eq. (1) are given in Table I.

TABLE I. Parameters (in atomic units) in the site–site potential of Eq. (1).

	A_{ij}	B_{ij}	q_iq_j	C_{ij}	r_{ij}^0
N–N	53.3531	1.5854	1.741 61	28.592 37	5.671 08
N–H	4.6253	1.8185	−0.580 54	10.811 17	5.103 97
H–H	1.1390	1.7617	0.193 51	4.289 51	4.536 86

Sagarik, Ahlrichs, and Brode conclude that the minimum of their potential is at the unsymmetrical cyclic structure, found experimentally by Nelson *et al.*[2,3,8] The depth of this minimum is -12.96 kJ mol^{-1} for the *ab initio* calculations and -10.79 kJ mol^{-1} when calculated from the site–site potential. However, when we scanned the entire site–site potential-energy surface, we found a deeper minimum (-11.86 kJ mol^{-1}) at a structure with a nearly linear hydrogen bond ($\vartheta_A=22°$, $\vartheta_B=71°$, $\varphi_A=\varphi_B=0°$, $\gamma=180°$, and $R=3.38$ Å). This structure was not one of the five dimer geometries investigated *ab initio*, and is about 1.07 kJ mol^{-1} more stable than the structure proposed by Sagarik, Ahlrichs, and Brode. A similar equilibrium structure was found by Hassett, Marsden, and Smith[5] who also performed *ab initio* calculations, but used seven different geometries and optimized 11 geometrical parameters by gradient techniques. The 11 parameters varied in this optimization are four N–H distances, four H–N–H angles, R, ϑ_A, and ϑ_B. It was assumed that two pairs of N–H distances and H–N–H angles are equal. Hassett, Marsden, and Smith also made an estimate of the barrier in the interchange tunneling path and arrived at a value of 29 cm^{-1}. We have also calculated this barrier. For given values of ϑ_A and ϑ_B, we calculated the site–site potential while relaxing all other coordinates to arrive at the minimum energy. The interchange tunneling path is the path of minimum energy from one minimum to the other and will be discussed in more detail below. For the site–site potential, a barrier of 77 cm^{-1} is found for this path.

In order to use the site–site intermolecular potential in the calculation of the VRT levels we find it convenient to expand it in a complete set of angular functions,[9]

$$V_{\rm int}(R,\gamma_A,\vartheta_A,\varphi_A,\gamma_B,\vartheta_B,\varphi_B)=\sum_{\Lambda}v_\Lambda(R)A_\Lambda(\gamma_A,\vartheta_A,\varphi_A,\gamma_B,\vartheta_B,\varphi_B), \tag{2a}$$

$$A_\Lambda(\gamma_A,\vartheta_A,\varphi_A,\gamma_B,\vartheta_B,\varphi_B)=\sum_M\begin{pmatrix}L_A & L_B & L\\ M & -M & 0\end{pmatrix}D^{(L_A)*}_{MK_A}(\gamma_A,\vartheta_A,\varphi_A)\times D^{(L_B)*}_{-MK_B}(\gamma_B,\vartheta_B,\varphi_B), \tag{2b}$$

where Λ stands for the set of quantum numbers (L_A,K_A,L_B,K_B,L), D denotes a Wigner rotation function, and the quantity in large parentheses denotes a Wigner $3j$ symbol. The potential depends only on the angles that relate the monomer frames to the dimer frame and on the van der Waals bond length. The expansion had to be truncated at

Downloaded 13 Jun 2006 to 128.32.220.140. Redistribution subject to AIP license or copyright, see http://jcp.aip.org/jcp/copyright.jsp

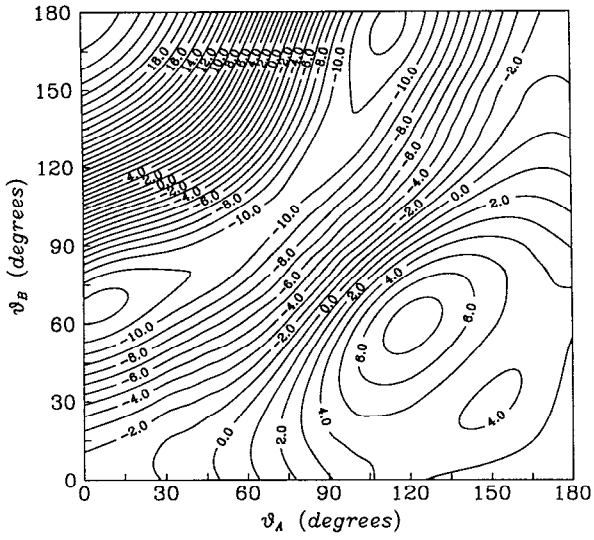

FIG. 1. Cut through the expanded potential, relaxing the coordinates φ_A, φ_B, γ, and R to obtain minimum energy for given values of ϑ_A and ϑ_B. The variation of R is restricted to the integration grid points between 2.78 and 4.18 Å. The numbers indicating the contour lines are energies in kJ mol^{-1}. See the text for a description of the interchange tunneling path.

$L_A, L_B = 5$, because an expansion to higher order would be too time consuming. The time needed to compute the VRT levels (see Sec. III) depends linearly on the number of terms retained in the spherical expansion. The truncated expansion reproduces the site–site potential to within about 8%. The minimum in the expanded potential occurs at a structure with a linear hydrogen bond ($\vartheta_A = 0°$, $\vartheta_B = 65°$, $\varphi_A = \varphi_B = 0°$, $\gamma = 180°$, and $R = 3.28$ Å), with a depth of -12.22 kJ mol^{-1} ($D_e = 1022$ cm^{-1}). The interchange tunneling path for the expanded potential has been calculated as described above for the site–site potential. In Fig. 1 we show the expanded potential along this path. When we follow the path starting from the minimum ($\vartheta_A = 0°$, $\vartheta_B = 65°$, $\varphi_A = \varphi_B = 0°$, $\gamma = 180°$), we go through a cyclic transition state ($\vartheta_A = 75°$, $\vartheta_B = 105°$, $\varphi_A = 60°$, $\varphi_B = 0°$, $\gamma = 180°$), to the other minimum at ($\vartheta_A = 115°$, $\vartheta_B = 180°$, $\varphi_A = \varphi_B = 60°$, $\gamma = 180°$). The value of R only changes by about 0.02 Å during this motion. A barrier of 167 cm^{-1} is found in this case. Hence, this barrier is very sensitive to the truncation of the spherical expansion, but the error in the barrier (167 cm^{-1} vs 77 cm^{-1}) is still within the indicated range of ±8% of the well depth of 1022 cm^{-1}. In Sec. V we will elaborate on the relation between this barrier and the interchange tunneling splitting in $(NH_3)_2$. We have also examined the barriers for rotation of the NH_3 monomers around their C_3 axes, and find that these are only slightly affected by the truncation of the spherical expansion of the potential.

The expansion coefficients $v_\Lambda(R)$ can be obtained by multiplying Eq. (2a) with one of the functions A_Λ and integrating over five angles.[9] Due to the symmetry of the problem (see Sec. IV) we can reduce the integration intervals. We have used a six-point Gauss–Legendre quadrature for the angles ϑ_A and ϑ_B on the interval $[0,\pi]$, a six-point Gauss–Chebyshev quadrature for the dihedral angle γ on the interval $[0,\pi]$, and a five-point Gauss–Chebyshev quadrature for the angles φ_A and φ_B on the interval $[0,2\pi/3]$. The number of expansion coefficients to be calculated can also be reduced by symmetry. All coefficients are real, and both K_A and K_B have to be multiples of three. Furthermore, it is easy to prove that

$$v_{L_B,K_B,L_A,K_A,L}(R) = (-1)^{L_A+L_B} v_{L_A,K_A,L_B,K_B,L}(R),$$
$$v_{L_B,-K_B,L_A,-K_A,L}(R) = (-1)^{L+K_A+K_B} v_{L_A,K_A,L_B,K_B,L}(R). \quad (3)$$

III. CALCULATION OF THE VIBRATION–ROTATION–TUNNELING LEVELS

If we use the coordinate system defined in Sec. II, the van der Waals Hamiltonian describing VRT motion in $(^{14}NH_3)_2$ can be written as[10]

$$\hat{H}_{\rm vdW} = \sum_\lambda A_\lambda(\hat{j}_{A\lambda}^2 + \hat{j}_{B\lambda}^2) + \frac{1}{2\mu R^2}(\hat{J}^2 + \hat{j}^2 - 2\hat{\mathbf{j}}\cdot\hat{\mathbf{J}}) - \frac{\hbar^2}{2\mu R}\frac{\partial^2}{\partial R^2}R + \sum_\Lambda v_\Lambda(R) \times A_\Lambda(\gamma_A,\vartheta_A,\varphi_A,\gamma_B,\vartheta_B,\varphi_B). \quad (4)$$

The Hamiltonian $\hat{H}_{\rm vdW}$ consists of four terms. The first term contains both rigid-rotor Hamiltonians of the monomers, with the body-fixed angular momenta $\hat{\mathbf{j}}_A$ and $\hat{\mathbf{j}}_B$. The rotational constants are taken as $A_x = A_y = 9.945$ cm^{-1} and $A_z = 6.229$ cm^{-1}, which are the mean values of the rotational constants for the 0^+ and 0^- umbrella states given in Ref. 11. The second term describes the overall rotation of the dimer and the Coriolis interaction; the operator $\hat{\mathbf{j}}$ is defined as $\hat{\mathbf{j}} = \hat{\mathbf{j}}_A^{\rm SF} + \hat{\mathbf{j}}_B^{\rm SF}$, where $\hat{\mathbf{j}}_A^{\rm SF}$ and $\hat{\mathbf{j}}_B^{\rm SF}$ are the space-fixed counterparts of $\hat{\mathbf{j}}_A$ and $\hat{\mathbf{j}}_B$. In the present work we have used the so-called helicity decoupling approximation. This means that we have neglected the small off-diagonal Coriolis contribution contained in the term $\hat{\mathbf{j}}\cdot\hat{\mathbf{J}}/\mu R^2$ and that Ω, the component of $\mathbf{j}$ as well as $\mathbf{J}$ on the dimer z axis, becomes a good quantum number. In calculations on Ar–NH_3 we have found[6] that the effect of this approximation on the VRT states is very small. The third term is the kinetic energy belonging to the radial coordinate R, with μ denoting the reduced mass of the complex. With the values[12] $m_H = 1.0078$ amu and $m_N = 14.0031$ amu for the masses of hydrogen and nitrogen, respectively, we get $\mu = 8.5133$ amu. The last term is the intermolecular potential as discussed in Sec. II.

In order to find a convenient basis for the diagonalization of $\hat{H}_{\rm vdW}$, we first diagonalized the Hamiltonian $\hat{H}_{\rm rad}$ defined by

$$\hat{H}_{\rm rad} = -\frac{\hbar^2}{2\mu R}\frac{\partial^2}{\partial R^2}R + V_{\rm rad}(R). \quad (5)$$

The radial potential $V_{\rm rad}(R)$ is found by fixing all angles to the values at the minimum of the expanded potential (see Sec. II) and varying R. The radial Hamiltonian $\hat{H}_{\rm rad}$ is diagonalized by taking a Morse-type basis[13] of six functions parametrized by $D_{\rm Morse} = 1021.2$ cm^{-1}, $R_{\rm Morse} = 3.55$ Å, and $\omega_{\rm Morse} = 108$ cm^{-1}. All integrations over the coordi-

Downloaded 13 Jun 2006 to 128.32.220.140. Redistribution subject to AIP license or copyright, see http://jcp.aip.org/jcp/copyright.jsp

nate R were performed by using a 12-point Gauss–Laguerre quadrature.

We calculate the bound states of the Hamiltonian $\hat{H}_{\rm vdW}$ [Eq. (4)] by using the symmetry-adapted (see Sec. IV) combinations of the basis functions,[10]

$$|j_A,k_A j_B,k_B j,\Omega,J,M,n\rangle$$

$$=\left[\frac{(2j_A+1)(2j_B+1)(2J+1)}{256\pi^5}\right]^{1/2}$$

$$\times\sum_{\Omega_A,\Omega_B} D^{(j_A)*}_{\Omega_A k_A}(\gamma_A,\vartheta_A,\varphi_A) D^{(j_B)*}_{\Omega_B k_B}(\gamma_B,\vartheta_B,\varphi_B)$$

$$\times\langle j_A\Omega_A j_B\Omega_B|j\Omega\rangle D^{(J)*}_{M\Omega}(\alpha,\beta,0)\varphi_n(R), \qquad (6)$$

where the quantity in angular brackets denotes a Clebsch–Gordan coefficient.The functions $\varphi_n(R)$ $(n=1,2,3)$ are the lowest three eigenfunctions of the radial Hamiltonian $\hat{H}_{\rm rad}$ of Eq. (5) and are contractions of the Morse-type basis functions described above.

We have chosen $j_{\max}=5$ for the maximum values included for the rotational quantum numbers j_A and j_B of the monomers. This limit is imposed by computer resources. It should be noted that with this set of basis functions the energy levels are not fully converged. The energy differences have converged better, however, and we expect the ordering of the levels within the energy-level scheme to be correct for the intermolecular potential used. For the states possessing A-type symmetries (see Sec. IV), we were able to perform calculations with $j_{\max}=6$. This gives us an estimate of the error of the energies calculated. The average lowering in the absolute energies of the levels going from $j_{\max}=5$ to $j_{\max}=6$ is 20 $\rm cm^{-1}$. The average changes in the energy differences are about 15%.

IV. SYMMETRY

From the neglect of the NH_3 inversion tunneling and the assumption of low barrier internal rotation and interchange motions,[8] we arrive at G_{36} as the molecular symmetry (MS) group[14] for the NH_3 dimer. We label the atoms in monomer A, 1–3 (^{1}H, $I=1/2$) and 7 (^{14}N, $I=1$). The atoms in monomer B are labeled 4–6 (^{1}H) and 8 (^{14}N). Nelson and Klemperer[8] have in fact used that G_{36} is isomorphic to the semidirect product $(C_3^A\otimes C_3^B)\wedge(C_2\otimes C_s)$, in which C_3^A and C_3^B contain the cyclic permutations of the protons in monomers A and B, respectively. We find it more convenient to group these permutations into "geared" and "antigeared" permutations of both monomers simultaneously and use the relation that G_{36} is a direct product of two commuting groups $G_{36}\simeq C_{3v}^{\rm ag}\otimes C_{3v}^{\rm g}$ (see Table V). The group $C_{3v}^{\rm ag}$ is generated by the antigeared permutation $\hat{R}_1=(123)(465)$ and the monomer interchange permutation $\hat{I}_1=(14)(25)(36)(78)$, and the group $C_{3v}^{\rm g}$ by the geared permutation $\hat{R}_2=(123)(456)$ and the interchange operation $\hat{I}_2=(14)(26)(35)(78)^*$; the latter operation includes space inversion, $\hat{E}^*$, in order to preserve the handedness of the NH_3 monomers. The advantage of using this direct product separation is that the irreducible representations (irreps) of G_{36} can be directly obtained by Kronecker matrix multiplication of the irreps of the group C_{3v}. The difference with the treatment by Nelson and Klemperer[8] is only mathematical, however, We do not imply that the geared and antigeared rotations of the monomers are less hindered than the separate monomer rotations.

TABLE II. Transformation properties of the basis functions of Eq. (6).

Generator	Effect on basis
$\hat{R}_1=(123)(465)$	$\exp[2\pi i(k_A-k_B)/3]\ \|j_A k_A j_B k_B j\Omega JMn\rangle$
$\hat{I}_1=(14)(25)(36)(78)$	$(-1)^{J+j_A+j_B}\ \|j_B k_B j_A k_A j-\Omega JMn\rangle$
$\hat{R}_2=(123)(456)$	$\exp[2\pi i(k_A+k_B)/3]\ \|j_A k_A j_B k_B j\Omega JMn\rangle$
$\hat{I}_2=(14)(26)(35)(78)^*$	$(-1)^{j+k_A+k_B}\ \|j_B-k_B j_A-k_A j\Omega JMn\rangle$

The action of the group generators on the basis functions of Eq. (6) is given in Table II. In the Appendix we describe the construction of a spatial basis that spans the irreps of G_{36} and is adapted to a subgroup chain. Also, the combination with the ^{1}H and ^{14}N nuclear-spin functions is treated in the Appendix. This is required, not only for the derivation of the nuclear-spin statistical weights, but also for the calculation of the expectation values of operators, especially when these are nuclear-spin dependent, such as the ^{14}N quadrupole coupling with the electric-field gradient. For comparison with infrared and microwave spectra, it is important to know that the dipole operator belongs to the A_3 irrep of G_{36}, which yields the following selection rules:

$$A_1\leftrightarrow A_3,\quad A_2\leftrightarrow A_4,\quad E_1\leftrightarrow E_2,\quad E_3\leftrightarrow E_3,\quad E_4\leftrightarrow E_4,\quad G\leftrightarrow G. \qquad (7)$$

The symmetry adaptation of the basis is not only a matter of convenience. It reduces the size of the calculations significantly and, in this case, it was essential to make the calculation of the VRT levels possible. In the helicity decoupling approximation the effective symmetry is higher: $C_\infty\wedge G_{36}$, with the quantum number Ω labeling the irreps of C_∞. This approximate symmetry appears to be very useful for understanding the results of the calculations, as well as for the interpretation of the experimental data.

TABLE III. Energies (in $\rm cm^{-1}$) of the VRT states $|\Gamma\upsilon J|\Omega|\rangle$ in $(NH_3)_2$.

$\|A_1000\rangle-549.3158$	$\|E_1011\rangle-541.0893$	$\|G000\rangle-546.2754$
$\|A_2010\rangle-548.9978$	$\|E_3011\rangle-538.8871$	$\|G010\rangle-545.9570$
$\|A_4000\rangle-543.7598$	$\|E_4011\rangle-538.8871$	$\|G100\rangle-530.4652$
$\|A_3010\rangle-543.4418$	$\|E_1100\rangle-535.7633$	$\|G110\rangle-530.1472$
$\|A_1111\rangle-539.0259$	$\|E_1110\rangle-535.4453$	
$\|A_2111\rangle-539.0259$	$\|E_2011\rangle-535.2582$	
$\|A_3111\rangle-532.7363$	$\|E_3100\rangle-533.2064$	
$\|A_4111\rangle-532.7363$	$\|E_4110\rangle-532.8883$	
	$\|E_2100\rangle-528.6631$	
	$\|E_2110\rangle-528.3453$	
	$\|E_4200\rangle-525.2624$	
	$\|E_3210\rangle-524.9446$	

Downloaded 13 Jun 2006 to 128.32.220.140. Redistribution subject to AIP license or copyright, see http://jcp.aip.org/jcp/copyright.jsp

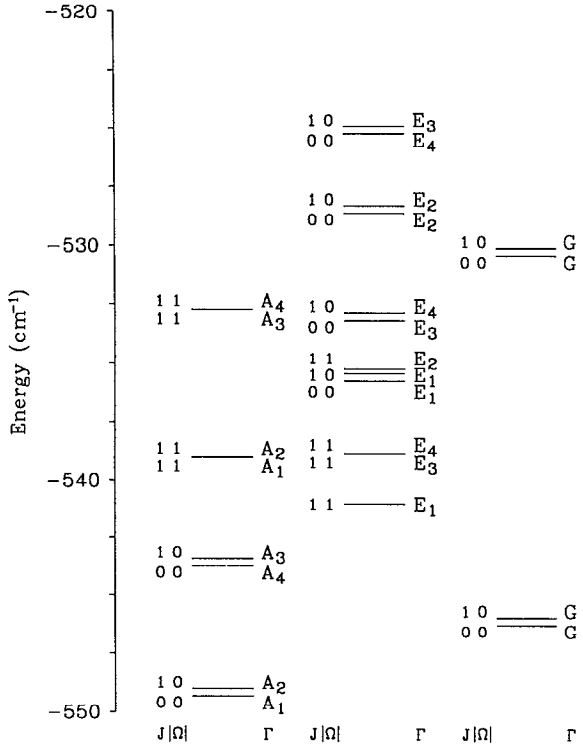

FIG. 2. Computed VRT levels of $(NH_3)_2$. All states with $J=0$ and $J=1$ that lie below -520 cm^{-1} are shown, except for the states of G symmetry with $J=|\Omega|=1$ (see text).

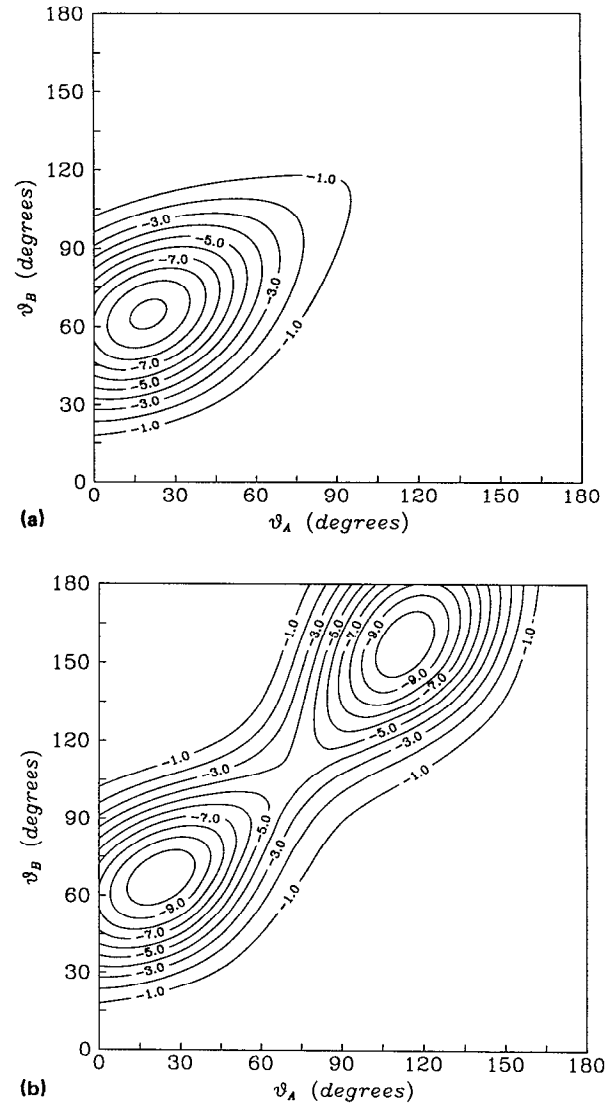

FIG. 3. Cut through the wave function of the state $|A_1000\rangle$, (a) with fixed (equilibrium) values $\varphi_A=\varphi_B=0°$, $\gamma=180°$, and $R=3.28$ Å; and (b) along the interchange tunneling path of Fig. 1 as explained in the text.

V. RESULTS AND DISCUSSION

In Table III and Fig. 2 we show the VRT levels calculated. We label the van der Waals states by $|\Gamma v J|\Omega|\rangle$, where J and Ω are the overall rotational quantum number and the helicity, Γ is an irrep of G_{36} labeling the spatial part of the wave function, and v is a label for the different states belonging to the same irrep. In this notation we have suppressed all nuclear-spin quantum numbers, which are accounted for by the nuclear-spin statistical weights. The operator $\hat{j}_z$ is a constant of the motion, because the helicity decoupling approximation is used. Since $\hat{I}_1$ does not commute with $\hat{j}_z$, it follows that the direct sums of G_{36} irreps $A_1 \oplus A_2$, $A_3 \oplus A_4$, and $E_3 \oplus E_4$ are irreducible under $C_\infty \wedge G_{36}$, i.e., that all states with $\pm\Omega$ are degenerate. In reality, the $|\Omega|=1$ states in Fig. 2 which belong to different G_{36} irreps will be slightly split by off-diagonal Coriolis interactions.

These calculations put high demands on the computer resources. To give some impression, the calculation of the $J=\Omega=0$ states of G symmetry took nearly 20 CPU hours on the IBM 3090/600. The Hamiltonian matrix had a dimension of 2694 in this case. For the $J=|\Omega|=1$ states of E_1 symmetry the dimension is 2796 and the time to compute the energies was nearly 30 CPU hours. It was found that the construction of the Hamiltonian matrix was the most time-consuming step.

Our first point of interest concerns the dissociation energies D_0 of the different nuclear-spin species. For *ortho* NH_3, the ground state is the $j=k=0$ monomer state. The ground state of the *para* NH_3 monomer is the $j=|k|=1$ state. Dimer states of A symmetry dissociate into two *ortho* NH_3 monomers, states of E symmetry into two *para* NH_3 monomers, and states of G symmetry into one *ortho* and one *para* NH_3 monomer (see Table VI). The dissociation energies, relative to the ground states of the dissociation products, are 549.3, 573.4, and 562.8 cm^{-1}, for the ground states of A, E, and G symmetry, respectively. Therefore, the species corresponding to E symmetry is the most stable. This may be expected because *para* NH_3 monomers with $j=|k|=1$ are more easily orientationally localized by the anisotropic dimer potential than *ortho* NH_3 monomers with $j=k=0$. Also, the absolute ground-state energies (see Table III) are different, which is noteworthy because it indicates that the NH_3 dimer is not a rigid molecule.

Figures 3(a) and (b) show cuts through the wave functions of the $|A_1000\rangle$ state. In Fig. 3(a) all coordinates except ϑ_A and ϑ_B are frozen at the values in the minimum

Downloaded 13 Jun 2006 to 128.32.220.140. Redistribution subject to AIP license or copyright, see http://jcp.aip.org/jcp/copyright.jsp

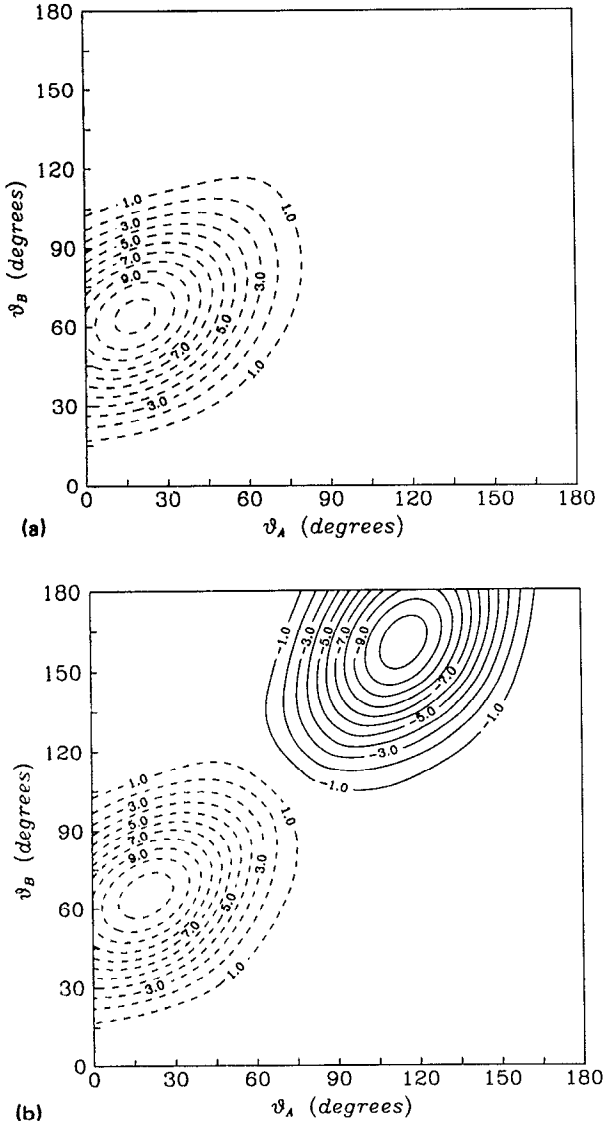

FIG. 4. Cut through the wave function of the state $|A_4000\rangle$, (a) with fixed (equilibrium) values $\varphi_A=\varphi_B=0°$, $\gamma=180°$, and $R=3.28$ Å; and (b) along the interchange path of Fig. 1 as explained in the text.

of the expanded potential, i.e., $\varphi_A=\varphi_B=0°$, $\gamma=180°$, and $R=3.28$ Å. We observe that the position of the maximum in the vibrational wave function ($\vartheta_A\approx 20°$ and $\vartheta_B\approx 65°$) does not coincide with the minimum in the potential. However, from this figure we cannot determine whether interchange tunneling takes place. In Fig. 3(b) we followed the wave function along the interchange tunneling path of minimum energy which passes through a cyclic structure (see Sec. II). The coordinates at which the wave function was calculated are the same as those at which we have plotted the expanded potential in Fig. 1. This means that not only the coordinates ϑ_A and ϑ_B vary, but implicitly also the coordinates φ_A, φ_B, γ, and R. Figures 4(a) and 4(b) show the same information for the $|A_4000\rangle$ state. From these figures it is clear that these two states form an interchange tunneling doublet. The associated energy splitting of 5.6 cm^{-1} shows that the interchange is indeed a feasible operation. The extent to which vibrational averaging takes place is very sensitive to the barrier in the interchange tunneling path. In our expanded potential this barrier is too high. This means that we probably underestimate the splitting between these two levels, and hence also the effects of the vibrational averaging.

The two minima in the expanded potential shown in Fig. 1 are connected by the symmetry operation $\hat{R}_2\hat{I}_2$. If interchange tunneling were not a feasible operation, the MS group would become G_{18} with $\hat{R}_1$, $\hat{R}_2$, and $\hat{I}_1\hat{I}_2$ as generators.[8] The generator $\hat{I}_1\hat{I}_2$ of G_{18} is a product of two interchange operations, one of which is combined with space inversion. It corresponds to a reflection with respect to a plane containing the dimer axis, and not to an interchange operation. The irreps A_1 and A_4 of G_{36} both correlate to the irrep A_1 of G_{18}. This gives us a group-theoretical confirmation that the splitting between the A_1 and A_4 levels found above is indeed due to interchange tunneling.

From Fig. 2 and the selection rules of Eq. (7) it can be seen that the states of G symmetry support pure rotational transitions. The microwave experiments of Nelson *et al.*[2,3] probed only these states. Their experiments show that two states with $J=\Omega=0$ (called G_α and G_β in Refs. 2 and 3) are very close in energy. Nelson *et al.* infer from the microwave and infrared measurements by Fraser *et al.*[7] that neither NH_3 monomer is inverting, hence they conclude that these states belong to different van der Waals vibrations. From the properties of these two G states they deduce that the interchange tunneling is nearly quenched.

The principal result from the microwave experiments of Nelson *et al.*[2,3] is the structure of the NH_3 dimer. The rotational constants are found[2] to be $B_\alpha=5110.412(2)$ MHz and $B_\beta=5110.564(2)$ MHz for the G_α and G_β states, respectively. From the rotational constants the separation between the centers of mass was calculated as $R_{CM}=3.3374(1)$ Å. By taking half the energy difference between the calculated $|G000\rangle$ and the $|G010\rangle$ states (see Table III), we arrive at a rotational constant of $B=4772.7$ MHz and a distance $R_{CM}=3.53$ Å, in fairly good agreement with experiment. From the centrifugal distortion constant, Nelson *et al.*[3] obtained an estimate of the van der Waals stretching frequency $\omega_s=106(1)$ cm^{-1}, within the pseudodiatomic approximation. Our calculated stretching frequency $\omega_s=108$ cm^{-1} is very close to this estimate. From a harmonic calculation, Dykstra and Andrews[15] found a stretching frequency of 160 cm^{-1}, which deviates substantially from the value of Nelson *et al.* and from our value.

Information on the angles ϑ_A and ϑ_B can be obtained from both the ^{14}N quadrupole splittings and from the measured value of the dipole moment of the dimer. When the nuclear quadrupole interaction is taken into account the Hamiltonian can be written as

$$\hat{H}=\hat{H}_{vdW}+\hat{H}_Q^A+\hat{H}_Q^B, \tag{8}$$

where $\hat{H}_{vdW}$ is the van der Waals Hamiltonian of Eq. (4) and $\hat{H}_Q^X$ ($X=A,B$) are the quadrupole interaction Hamiltonians of the monomers A and B. The quadrupole interaction Hamiltonian $\hat{H}_Q^X$ is an inner product of two tensor operators, one acting on the spatial wave functions and one

Downloaded 13 Jun 2006 to 128.32.220.140. Redistribution subject to AIP license or copyright, see http://jcp.aip.org/jcp/copyright.jsp

acting on the nuclear-spin part. Following Nelson *et al.*[2,3] we assume that the field gradient at the nitrogen nucleus of a monomer is not altered by the presence of the other monomer. Although we suppressed the nuclear-spin quantum numbers in our notation of the eigenkets, they correspond to Pauli allowed total wave functions. These are obtained by projecting the A_2 component of P_{18} (see the Appendix) out of the tensor product $\Gamma \otimes \Gamma^{\text{spin}}$, where Γ and Γ^{spin} are irreps of G_{36}, belonging to the spatial and nuclear-spin part, respectively. The quadrupole splitting can be obtained by first-order perturbation theory with the operator $\hat{H}_Q^A + \hat{H}_Q^B$ on the eigenstates of $\hat{H}_{\text{vdW}}$.

It is shown in the Appendix that for states with A or E symmetry the quadrupole splitting calculated in this way depends only on one average quadrupole coupling constant. For states with G symmetry, which arise from the coupling of an *ortho* and a *para* monomer, two *different* quadrupole coupling constants are obtained. These constants may be calculated from those (primitive) basis functions of Eq. (6) that transform according to $\Gamma = G$. From the derivation in the Appendix it follows that for $\Omega = 0$ one quadrupole coupling constant is proportional to the expectation value $\langle P_2(\cos \vartheta_o)\rangle$ of the *ortho* monomer and the other constant is proportional to the same quantity $\langle P_2(\cos \vartheta_p)\rangle$ of the *para* monomer. The expectation value of the dipole operator with respect to an $\Omega = 0$ state of G symmetry vanishes because of space inversion symmetry. Switching on an external field lowers the symmetry to P_{18}; from the observed second-order Stark splitting of the $\Omega = 0$ states one can deduce the quantity $\langle P_1(\cos\vartheta_o)\rangle + \langle P_1(\cos \vartheta_p)\rangle$.

Nelson, Fraser, and Klemperer[2] have indeed found two different values of $\langle P_2(\cos\vartheta)\rangle$. They could not assign these values to the *ortho* or *para* monomers, but we find the best agreement with our calculations for the ground state of G symmetry if we assume that their monomer A is the *ortho* species and monomer B the *para* species. From their values of $\langle P_2(\cos \vartheta)\rangle$ Nelson, Fraser, and Klemperer[2] conclude that the "average" angles are $\vartheta_A = 48.6(1)°$ or $131.4(1)°$ and $\vartheta_B = 64.5(1)°$ or $115.5(1)°$. The component of the dimer dipole moment μ along the dimer bond axis is given by

$$\mu = \mu_0[\langle P_1(\cos \vartheta_A)\rangle + \langle P_1(\cos \vartheta_B)\rangle] + \mu^{\text{ind}}, \tag{9}$$

where $\mu_0 = -1.47$ D (Ref. 16) is the dipole moment of an NH_3 monomer. Following Nelson *et al.*[2,3] we assume that the monomer dipole moments do not change upon dimer formation, other than by induction. The induced dipole moment μ^{ind} along the dimer bond axis can be approximated by

$$\mu^{\text{ind}} = 2\alpha\mu_0 R_{\text{CM}}^{-3}[\langle P_1(\cos \vartheta_A)\rangle + \langle P_1(\cos \vartheta_B)\rangle], \tag{10}$$

where $\alpha = 13.95\ a_0^3$ (Ref. 17) is the dipole polarizability of the NH_3 monomer (which is nearly isotropic) and $R_{\text{CM}} = 3.53$ Å. From the measured dipole moment of the dimer $\mu = -0.75$ D and an assumed induced dipole moment of $\mu^{\text{ind}} = -0.3$ D, Nelson, Fraser, and Klemperer[2] conclude that the average angles are in fact $\vartheta_A = 48.6(1)°$ and $\vartheta_B = 115.5(1)°$.

From our calculations we have found the following values for the ground state of G symmetry:

$$\langle P_2(\cos \vartheta_o)\rangle = 0.4822, \quad \langle P_2(\cos \vartheta_p)\rangle = -0.2388 \tag{11a}$$

and

$$\langle P_1(\cos \vartheta_o)\rangle = 0.7595, \quad \langle P_1(\cos \vartheta_p)\rangle = 0.2356. \tag{11b}$$

Due to the truncation of our free-rotor basis, Eq. (6), these values have not fully converged. Upon extending the basis from $j_{\max} = 4$ to $j_{\max} = 5$, we found that the angles which can be obtained from these expectation values still changed by 5–10°, towards the equilibrium angles. The angles $\vartheta_o = 36.0°$ and $\vartheta_p = 65.3°$ obtained from the expectation values $\langle P_2(\cos \vartheta)\rangle$, Eq. (11a), are not inconsistent with the experimental values deduced from $\langle P_2(\cos \vartheta)\rangle$ only. However, using their dipole moment, Nelson *et al.* have chosen the value $\vartheta_B = 115.5°$, which does not agree with our value of ϑ_p. The (smaller) discrepancy between their value $\vartheta_A = 48.6°$ and our value $\vartheta_o = 36.0°$ may be due to the truncation error in the potential that we have used; for the unexpanded potential the equilibrium angle is $\vartheta_A = 22°$, whereas for the truncated expansion of the potential this equilibrium angle is $\vartheta_A = 0°$ (see Sec. II). The dipole moment calculated from Eq. (9) and (10) with the angles $\vartheta_o = 36.0°$ and $\vartheta_p = 65.3°$ obtained from $\langle P_2(\cos \vartheta)\rangle$ is $\mu = -1.97$ D ($\mu^{\text{ind}} = -0.17$ D). When we use our values of $\langle P_1(\cos \vartheta_o)\rangle$ and $\langle P_1(\cos \vartheta_p)\rangle$ directly, a dipole moment of $\mu = -1.60$ D ($\mu^{\text{ind}} = -0.14$ D) is found. This shows that one must use caution in calculating the dipole moment from the average angles obtained from $\langle P_2(\cos \vartheta)\rangle$. Our value of the vibrationally averaged dipole moment $\mu = -1.60$ D is substantially smaller than the dipole $\mu = -2.29$ D obtained for the equilibrium structure in the expanded potential, but still too large compared to the experimental value $\mu = -0.75$ D. The angles found from the expectation values $\langle P_1(\cos \vartheta_o)\rangle$ and $\langle P_1(\cos \vartheta_p)\rangle$ are $\vartheta_o = 40.6°$ and $\vartheta_p = 76.4°$, respectively. We note especially that the difference between the "average" angles $\vartheta_o = 40.6°$ and $36.0°$ calculated from $\langle P_1(\cos \vartheta_o)$ and $\langle P_2(\cos \vartheta_o)\rangle$, and the equilibrium angle $\vartheta_A = 0°$ is striking.

In Figs. 5(a) and 5(b) we show the probability amplitudes of the lowest two $J = 0$ states of G symmetry along the interchange tunneling path of Fig. 1. These pictures may be compared with Figs. 3(b) and 4(b), which show the A_1 and A_4 wave functions along the same path. It is clear that the states of G symmetry are much more localized. This can be understood from the inequivalence of the *ortho* and *para* monomers that constitute the states of G symmetry and the different barriers for rotation of the two monomers around their C_3 axes. If the monomer C_3 rotations are not completely hindered, this leads to an energy gap between the lowest two $J = 0$ states of G symmetry (cf. Fig. 2), even in the absence of interchange tunneling. This gap will be large for the equilibrium structure with a linear hydrogen bond, since the barrier for C_3 rotation of the proton acceptor molecule is very small in this geometry. Interchange tunneling couples the two states of G symme-

Downloaded 13 Jun 2006 to 128.32.220.140. Redistribution subject to AIP license or copyright, see http://jcp.aip.org/jcp/copyright.jsp

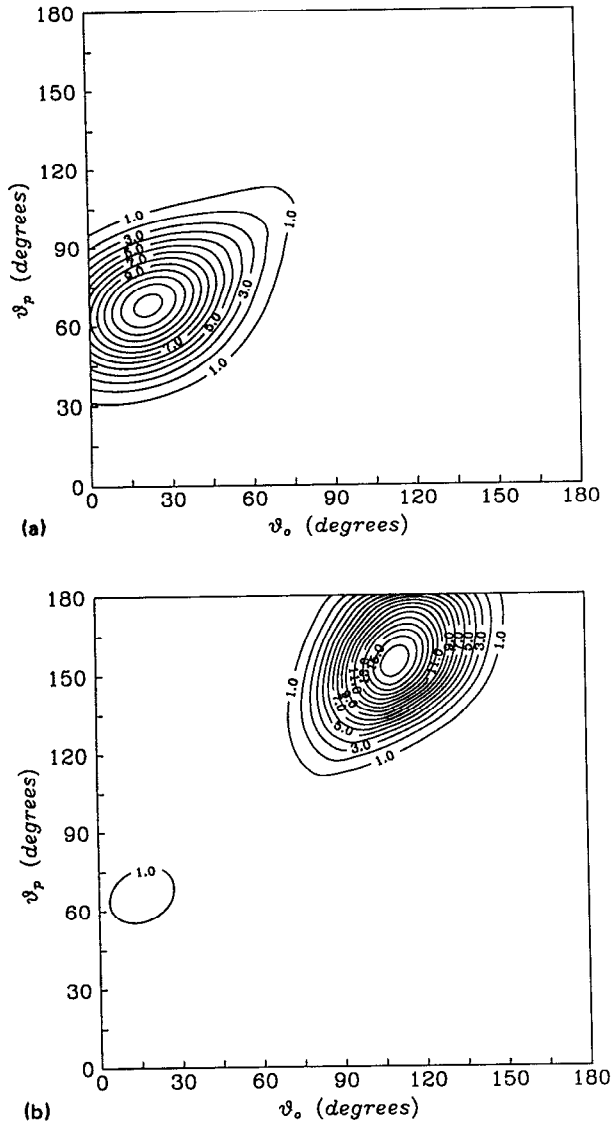

FIG. 5. Cuts through the probability distribution $|\Psi|^2$ of the states of G symmetry along the interchange tunneling path, cf. Figs. 3(b) and 4(b); (a) for the lowest state $|G0\,0\,0\rangle$ and (b) for the second state $|G1\,0\,0\rangle$.

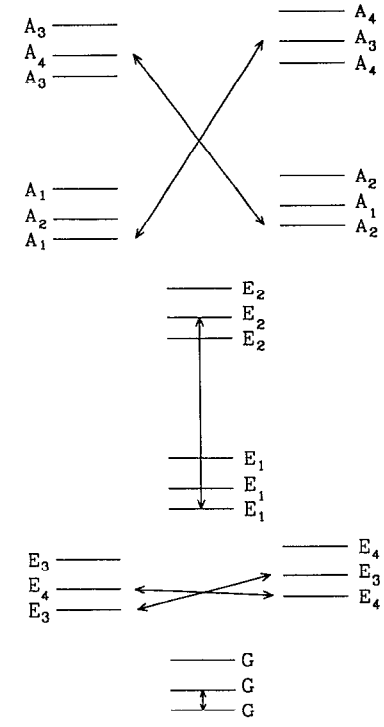

FIG. 6. Qualitative illustration of the rotational G_{36} ladders. The ladders on the left- and on the right-hand side are offset by Coriolis interaction; the ladders in the middle part of the drawing are not split by this interaction. For each species a typical allowed $\Delta J=1$ transition is indicated.

try and thereby increases their energy gap. On the other hand, it leads to a displacement of the monomer C_3 axes towards the cyclic structure, which reduces the difference in the barriers for monomer rotation and thereby decreases the energy gap. As displayed in Fig. 5, the wave functions show considerable amplitude away from the equilibrium structure, and in the higher state one may even observe the onset of interchange tunneling.

The states of G symmetry with $J=|\Omega|=1$ are not shown in Fig. 2, because we had to restrict our calculations for these states to $j_{max}=4$, while all the levels displayed in Fig. 2 have been calculated with $j_{max}=5$. By comparison with the results for $J=\Omega=0$, also calculated with $j_{max}=4$, we estimate that the lowest $J=|\Omega|=1$ state lies nearly 8 cm^{-1} below the lowest $J=\Omega=0$ state. This does not agree with the microwave[2,20] and far-infrared[20] data. We believe that this discrepancy is related to the fact that we still underestimate the interchange tunneling in our calculations.

If we look at Fig. 2 and the selection rules of Eq. (7), it seems that the G states are not the only ones that support pure rotational transitions. The $J=|\Omega|=1$ states of E_3 and E_4 symmetry in Fig. 2 are degenerate. The states with higher J corresponding to the E_3 state will have E_3 symmetry for all odd J, but E_4 symmetry for even J, while the rotational levels of the E_4 state with $J=|\Omega|=1$ will have E_4 symmetry for all odd J, but E_3 symmetry for even J. Hence, the dipole selection rules $E_3 \leftrightarrow E_3$ and $E_4 \leftrightarrow E_4$ allow transitions with $\Delta J=1$ within this twofold degenerate manifold which involve only pure rotational quanta. However, as it is explained in the first paragraph of Sec. V, the degeneracy of the E_3 and E_4 states is actually lifted by off-diagonal Coriolis interactions and the frequencies of these rotational transitions are shifted. In Ref. 20 these shifted rotational transitions have indeed been observed. The dipole matrix elements are explicitly discussed in the Appendix of the present paper, where it is shown also that the $|\Omega|\geqslant 1$ states of E_3, E_4, and G symmetry (and not those of other symmetries) will display a first-order Stark splitting. Measurement of these splittings will directly provide additional information on the dipole moment of the NH_3 dimer.

In Table IV the band origins of the published far-infrared transitions are given. By using combination differences it has been shown that transitions 2 and 8 share the same initial level.[18] Furthermore, transitions 4 and 5 share the initial states with the microwave transitions and are

Downloaded 13 Jun 2006 to 128.32.220.140. Redistribution subject to AIP license or copyright, see http://jcp.aip.org/jcp/copyright.jsp

TABLE IV. Experimental far-infrared transition frequencies (in GHz).

1	453.5995(1)[a]	$\|\Omega\|=1\rightarrow1$
2	483.301 07(6)[a]	$\|\Omega\|=0\rightarrow0$
3	486.7314(4)[a]	$\|\Omega\|=1\rightarrow1$
4	613.7202(3)[b]	$\|\Omega\|=0\rightarrow0$
5	614.6354(3)[b]	$\|\Omega\|=0\rightarrow0$
6	730.6045(2)[b]	$\|\Omega\|=1\rightarrow1$
7	730.5653(2)[b]	$\|\Omega\|=1\rightarrow1$
8	734.0586(4)[b]	$\|\Omega\|=0\rightarrow1$
9	747.0918(3)[b]	$\|\Omega\|=1\rightarrow1$

[a]From Ref. 18.
[b]From Ref. 19.

therefore G-type transitions.[19] Transitions 2 and 8 were shown to be A-type transitions.[19,20] Although our potential is not good enough to make definite assignments, we think that this assignment is correct. We assign the lines $|A_1000\rangle\rightarrow|A_3010\rangle$ at 176 GHz and $|A_1000\rangle\rightarrow|A_3111\rangle$ at 497 GHz to the $R(0)$ lines of transitions 2 and 8. This means that the interchange tunneling splitting for the states of A-type symmetry is known precisely [483.301 07(6) GHz]. We find a splitting of 176 GHz, which confirms that our barrier for the interchange tunneling is too high. The line $|G000\rangle\rightarrow|G110\rangle$ calculated at 484 GHz should correspond to the $R(0)$ line of transition 4 or 5, which is found experimentally at 614 GHz. The detailed experimental results and analysis presented by Loeser *et al.*[20] in the accompanying paper unambiguously confirm these statements and rigorously determine the tunneling splitting.

VI. CONCLUSIONS

We have calculated the VRT levels of the NH_3 dimer for $J=0$ and 1. For the intermolecular potential we used a spherical expansion of the site–site potential of Sagarik, Ahlrichs, and Brode,[4] which they have obtained from a fit to *ab initio* data. We can explain several features of the published microwave and far-infrared spectra and we feel that the results contribute much to the understanding of the dynamics of this complex.

We find that the lowest states of A_1 and A_4 symmetry are well separated in energy from other states of the same symmetry and form an interchange tunneling doublet. From the far-infrared data we conclude that the splitting between the A_1 and A_4 levels in our calculation is too small. This splitting is related to the barrier in the interchange tunneling path. The corresponding barrier (29 or 77 cm^{-1}) in the *ab initio* calculations of Refs. 4 and 5 may be realistic, but our truncated expansion of the potential overestimates this barrier (167 cm^{-1}). On the other hand, the truncation of the free-rotor basis may overestimate the amount of delocalization. If, however, we compare our results with those of Marshall, Jensen, and Bunker[21] for the HF dimer (where the basis was varied from $j_{max}=4$–10), we conclude that interchange tunneling occurs much more easily in $(NH_3)_2$ than in $(HF)_2$.

We have found that the vibrationally averaged structure calculated for the lowest state of G symmetry deviates substantially from the *ab initio* equilibrium structure. Our average structure is not the cyclic structure which Nelson *et al.*[2,3] deduced from the microwave spectrum, however. Taking into account that we underestimate the vibrational averaging because our barrier in the interchange tunneling path is too high, and that the minimum in the expanded potential deviates by 22° in ϑ_A from the minimum in the original site–site potential, we do believe that the experimental structure can be obtained from the *ab initio* equilibrium structure by vibrational averaging. Our *ortho* average value of $\vartheta_o\approx40°$ deviates considerably from the equilibrium angle ($\vartheta_A=0°$), but at this moment we cannot decide whether in reality the *para* average value of ϑ_p should be larger than 90°, as in the cyclic structure,[2] or smaller, as in our calculations, $\vartheta_p\approx70°$ (equilibrium value $\vartheta_B=65°$).

At this point we would like to elaborate on the nature of the states G_α and G_β, observed by Nelson *et al.*[2,3] Since these states are almost equally populated at a beam temperature of 1 K, they should lie very close together. According to Nelson *et al.* they correspond to two different van der Waals vibrations. We find a much larger splitting between the lowest states of G symmetry in our calculations, which is due to the different hindered rotations for the *ortho* and *para* monomers, as well as to interchange tunneling. This must imply that the two states G_α and G_β of Nelson *et al.* correspond in fact to our lowest state of G symmetry which in reality, but not in our calculations, is split by inversion tunneling. The results of Loeser *et al.*[20] in the accompanying paper establish that this is the case, and that this inversion is partly, but not completely, quenched in the NH_3 dimer. This (hindered) NH_3 monomer inversion may also reduce the effective dipole moment of the dimer and, thereby, diminish the gap which is still present between our calculated average dipole moment and the observed value.[2,3] It is also possible, however, that the "observed" value of the dipole moment is not completely correct, because Nelson *et al.* extracted this value from second-order Stark splitting, while neglecting the monomer inversion.

Finally, we discuss some qualitative pictures for the VRT dynamics of $(NH_3)_2$. Since the functions with different j_A, k_A and j_B, k_B in our free-rotor basis are strongly mixed and the eigenstates are to some extent localized, we exclude the free internal rotor limit. The other extreme, the nearly rigid limit, is excluded too, because of the large-amplitude motions along the interchange tunneling path and the substantial tunneling splitting between the A_1 and A_4 states. Moreover, the ground-state energies of the different nuclear-spin species are different. In Ref. 8 Nelson and Klemperer propose some other limiting cases. One limit is the $(2C_3+I)$ limit, wherein the interchange splitting is small compared with the splitting due to internal rotations around the C_3 axes. In the $(I+2C_3)$ limit it is just the other way around. Nelson and Klemperer argue that the $(2C_3+I)$ limit is the most likely. From the energy-level scheme (Fig. 2) we conclude that our results are intermediate between these two limits. If we account for the fact that we underestimate the interchange tunnel-

Downloaded 13 Jun 2006 to 128.32.220.140. Redistribution subject to AIP license or copyright, see http://jcp.aip.org/jcp/copyright.jsp

TABLE V. Groups of antigeared permutations C_{3v}^{ag} and geared permutations C_{3v}^{g}.

C_{3v}^{ag}	C_{3v}^{g}
C_3^{ag}: (1)	C_3^{g}: (1)
(123)(465)$=\hat{R}_1$	(123)(456)$=\hat{R}_2$
(132)(456)	(132)(465)
(14)(25)(36)(78)$=\hat{I}_1$	(14)(26)(35)(78)*$=\hat{I}_2$
(16)(24)(35)(78)	(15)(24)(36)(78)*
(15)(26)(34)(78)	(16)(25)(34)(78)*

ing splitting, we favor the $(I+2C_3)$ limit. This too is rigorously established by Loeser *et al.*, who, in the accompanying paper, describe the measurement and analysis of over 950 far-infrared VRT transitions and 12 microwave lines of $(NH_3)_2$. That work independently establishes the large interchange splitting in the states of A symmetry, the umbrella inversion of the constituent monomers, and the validity of the $(I+2C_3)$ limit for the internal motions of the dimer, and rigorously determines the energy-level diagram for all the lowest $\Omega=0$ and $|\Omega|=1$ levels.

ACKNOWLEDGMENTS

We thank Jennifer Loeser for her detailed and critical comments on this manuscript, Dr. W. Leo Meerts, Dr. Martina Havenith, and Harold Linnartz for valuable discussions, Professor Reinhart Ahlrichs for making available the parameters in the site–site potential of Ref. 4, IBM for granting computer time on the IBM 3090/600 at SARA (Amsterdam) and Rob Houweling from IBM for technical support. Part of this work has been performed as an IBM Academic Information Systems (ACIS) project. R.J.S. thanks the Research Institute of Materials (RIM) at Nijmegen for inviting him as a visiting professor. R.J.S. is supported by the National Science Foundation (Grant No. CHE86-12296).

APPENDIX

In this Appendix we will discuss the group-theoretical aspects of our computations. As stated in the main text, the pertinent permutation inversion group of two noninverting ammonia molecules is G_{36}, which is isomorphic to the outer direct product group $C_{3v}^{ag}\otimes C_{3v}^{g}$. The latter two commuting groups, consisting of "antigeared" and "geared" permutations, respectively, are listed in Table V. The Pauli principle is only concerned with permutations, not with inversion. We therefore remove the starred permutations from G_{36} and obtain a pure permutation group of order 18,

$$P_{18}\cong C_{3v}^{ag}\otimes C_3^{g}. \tag{A1}$$

The decomposition of the irreps (irreducible representations) of G_{36} under subduction to P_{18} is given in Table VI. The correlation rules follow simply from the observation that under the subduction $C_{3v}\downarrow C_3$ we have $A_2=A_1$ and $E=A_2\oplus A_3$. The same rules enable us to further subduce to the subgroup $C_3^{ag}\otimes C_3^{g}$, which obviously is isomorphic to the outer product $C_3^{A}\otimes C_3^{B}$, where $C_3^{A}=\{(1),(123),(132)\}$ and $C_3^{B}=\{(1),(456),(465)\}$. The correspondence between the irreps of $C_3^{ag}\otimes C_3^{g}$ and $C_3^{A}\otimes C_3^{B}$ is easily made by inspection of the characters of these isomorphic Abelian groups.

TABLE VI. Correlation diagram for irreps of G_{36}. Functions adapted to the given chain of subgroups are given. The short-hand notation: $|k_A,k_B\rangle\equiv|j_A\,k_A j_B k_B j\Omega JMn\rangle$ is used. The listed k values are unique mod 3. The action of $\hat{I}_1$ and $\hat{I}_2$ is given in Table II. The irreps of G_{36} are labeled according to Bunker (Ref. 14).

G_{36}	$\cong C_{3v}^{ag}\otimes C_{3v}^{g}$	$\supset C_{3v}^{ag}\otimes C_3^{g}$	$\cong P_{18}$	$\supset C_3^{ag}\otimes C_3^{g}$	$\cong C_3^{A}\otimes C_3^{B}$	Sequence adapted ket
A_1	$A_1\otimes A_1$	$A_1\otimes A_1$	A_1	$A_1\otimes A_1$	$A_1\otimes A_1$	$(\hat{E}+\hat{I}_1)(\hat{E}+\hat{I}_2)\|0,0\rangle$
A_2	$A_2\otimes A_1$	$A_2\otimes A_1$	A_2	$A_1\otimes A_1$	$A_1\otimes A_1$	$(\hat{E}-\hat{I}_1)(\hat{E}+\hat{I}_2)\|0,0\rangle$
A_3	$A_1\otimes A_2$	$A_1\otimes A_1$	A_1	$A_1\otimes A_1$	$A_1\otimes A_1$	$(\hat{E}+\hat{I}_1)(\hat{E}-\hat{I}_2)\|0,0\rangle$
A_4	$A_2\otimes A_2$	$A_2\otimes A_1$	A_2	$A_1\otimes A_1$	$A_1\otimes A_1$	$(\hat{E}-\hat{I}_1)(\hat{E}-\hat{I}_2)\|0,0\rangle$
E_1	$E\otimes A_1$	$E\otimes A_1$	E_1	$A_3\otimes A_1$	$A_2\otimes A_3$	$(\hat{E}+\hat{I}_2)\|1,-1\rangle$
				$A_2\otimes A_1$	$A_3\otimes A_2$	$(\hat{E}+\hat{I}_2)\hat{I}_1\|1,-1\rangle$
E_2	$E\otimes A_2$	$E\otimes A_1$	E_1	$A_3\otimes A_1$	$A_2\otimes A_3$	$(\hat{E}-\hat{I}_2)\|1,-1\rangle$
				$A_2\otimes A_1$	$A_3\otimes A_2$	$(\hat{E}-\hat{I}_2)\hat{I}_1\|1,-1\rangle$
E_3	$A_1\otimes E$	$A_1\otimes A_3$	A_3	$A_1\otimes A_3$	$A_2\otimes A_2$	$(\hat{E}+\hat{I}_1)\|1,1\rangle$
		$A_1\otimes A_2$	A_4	$A_1\otimes A_2$	$A_3\otimes A_3$	$(\hat{E}+\hat{I}_1)\hat{I}_2\|1,1\rangle$
E_4	$A_2\otimes E$	$A_2\otimes A_3$	A_5	$A_1\otimes A_3$	$A_2\otimes A_2$	$(\hat{E}-\hat{I}_1)\|1,1\rangle$
		$A_2\otimes A_2$	A_6	$A_1\otimes A_2$	$A_3\otimes A_3$	$(\hat{E}-\hat{I}_1)\hat{I}_2\|1,1\rangle$
G	$E\otimes E$	$E\otimes A_2$	E_2	$A_2\otimes A_2$	$A_2\otimes A_1$	$\|0,1\rangle$
				$A_3\otimes A_2$	$A_1\otimes A_2$	$\hat{I}_1\|0,1\rangle$
		$E\otimes A_3$	E_3	$A_2\otimes A_3$	$A_1\otimes A_3$	$\hat{I}_2\|0,1\rangle$
				$A_3\otimes A_3$	$A_3\otimes A_1$	$\hat{I}_2\hat{I}_1\|0,1\rangle$

Downloaded 13 Jun 2006 to 128.32.220.140. Redistribution subject to AIP license or copyright, see http://jcp.aip.org/jcp/copyright.jsp

Since a monomer spatial ket $|k_X=0\rangle$ belongs to A_1, a ket $|k_X=1\rangle$ to A_2, and a ket $|k_X=-1\rangle$ to A_3 of C_3^X, $X=A$ or B, the functions adapted to $C_3^{ag}\otimes C_3^g$ are simply products of spatial monomer kets of definite k values. If we further realize that kets adapted to A_1 and A_2 of C_{3v}^{ag} are, respectively, symmetric and antisymmetric under $\hat{I}_1$ and that the corresponding statement holds for C_{3v}^g and $\hat{I}_2$, all of Table VI follows easily. The spatial basis functions in this table are uniquely labeled by the irreps associated with the group chain $C_3^A\otimes C_3^B\subset P_{18}\subset G_{36}$. Henceforth we assume that all kets are adapted to this chain.

We define the monomer A proton spin functions such that

$$(123)\,|I_A,k_A,m_A\rangle=e^{i2\pi k_A/3}|I_A,k_A,m_A\rangle,$$

$$(23)\,|I_A,k_A,m_A\rangle=|I_A,-k_A,m_A\rangle. \tag{A2}$$

The same relations hold for the spin functions on B with (123) replaced by (456) and (23) by (56). The *ortho* proton spin functions are symmetric under all monomer permutations and hence transform as A_1 under C_3^X. They are designated as $|3/2,0,\ m_X\rangle$, $m_X=-3/2,\ldots,3/2$. The *para* functions $|1/2,1,m_X\rangle$ and $|1/2,-1,m_X\rangle$ span an A_2 and an A_3 irrep, respectively. Since $m_X=\pm 1/2$, the *para* functions carry two such irreps. We write, suppressing the magnetic quantum numbers of the proton functions,

$$|I_A,k_A;I_B,k_B\rangle=|I_A,k_A,m_A\rangle\otimes|I_B,k_B,m_B\rangle. \tag{A3}$$

The magnetic quantum numbers of the ^{14}N spin functions are explicitly shown: the spin function is written as $|M_N,M_N'\rangle$, where we suppress the I quantum numbers $(I_A=I_B=1)$. The following relations are the spin equivalents of two of the relations for spatial functions given in Table II:

$$\hat{I}_1|I_A,k_A;I_B,k_B\rangle\otimes|M_N,M_N'\rangle=|I_B,k_B;I_A,k_A\rangle\otimes|M_N',M_N\rangle,$$

$$\hat{I}_2|I_A,k_A;I_B,k_B\rangle\otimes|M_N,M_N'\rangle=|I_B,-k_B;I_A,-k_A\rangle\otimes|M_N',M_N\rangle. \tag{A4}$$

The last relation follows immediately from $\hat{I}_2=\hat{I}_1(23)(56)^*$, if we remember that spin is invariant under inversion and use Eq. (A2). The spin analogs of the relations for $\hat{R}_1$ and $\hat{R}_2$ in Table II follow easily from Eq. (A2). Table VII can now be derived by the same kind of considerations as were used for Table VI. The total number N of spin functions of different magnetic quantum number is given in the table. Although it may seem tempting to symmetry adapt the proton and nitrogen spin functions separately, followed by an adaptation of the product, this is not allowed, since P_{18} is not (isomorphic to) a product of two groups acting on the respective spin coordinates. Since the proton and nitrogen coordinates are intertwined in P_{18}, we must act on these coordinates simultaneously.

Since protons are fermions and ^{14}N nuclei are bosons, the total space-spin states must transform according to the antisymmetric representation A_2 of P_{18}. In order to construct such space-spin states, we must formally solve the Clebsch–Gordan (CG) problem of P_{18} (i.e., subduce irreps of $P_{18}\otimes P_{18}$ to P_{18}). Multiplicity-free CG coefficients can be calculated from irreducible f_λ-dimensional matrix irreps $\mathbf{U}(g)^\lambda$ by the following well-known formula, valid for an arbitrary finite group G:

$$\langle\lambda i\mu k\,|\,\nu q\rangle\langle\nu p\,|\,\lambda j\mu l\rangle=\frac{f_\nu}{|G|}\sum_{g\in G}U(g)_{ij}^{\lambda}U(g)_{kl}^{\mu}U(g^{-1})_{pq}^{\nu}. \tag{A5}$$

By the use of character relations it can be shown that the CG problem of P_{18} is indeed multiplicity free—see Table VIII—and since all the irreducible matrices $\mathbf{U}(g)^\lambda$ are known, the CG coefficients can be computed. The CG se-

TABLE VII. Spin functions adapted to P_{18} and G_{36}. The magnetic quantum numbers of the proton functions are suppressed in the dimer functions, but are accounted for in the spin statistical weight N. The second factor depends on the spin coordinates of ^{14}N, here the I quantum numbers are suppressed: $I_A=I_B=1$. The actions of $\hat{I}_1$ and $\hat{I}_2$ are given explicitly, cf. Table VI.

Spin function	N	P_{18}	G_{36}
$\|\frac{3}{2},0;\frac{3}{2},0\rangle\otimes\|M_N,M_N'\rangle+\|\frac{3}{2},0;\frac{3}{2},0\rangle\otimes\|M_N',M_N\rangle$	78	A_1	A_1
$\|\frac{3}{2},0;\frac{3}{2},0\rangle\otimes\|M_N,M_N'\rangle-\|\frac{3}{2},0;\frac{3}{2},0\rangle\otimes\|M_N',M_N\rangle$	66	A_2	A_4
$\|\frac{1}{2},1;\frac{1}{2},1\rangle\otimes\|M_N,M_N'\rangle+\|\frac{1}{2},1;\frac{1}{2},1\rangle\otimes\|M_N',M_N\rangle$	21	A_3	E_3
$\|\frac{1}{2},-1;\frac{1}{2},-1\rangle\otimes\|M_N,M_N'\rangle+\|\frac{1}{2},-1;\frac{1}{2},-1\rangle\otimes\|M_N',M_N\rangle$	21	A_4	E_3
$\|\frac{1}{2},1;\frac{1}{2},1\rangle\otimes\|M_N,M_N'\rangle-\|\frac{1}{2},1;\frac{1}{2},1\rangle\otimes\|M_N',M_N\rangle$	15	A_5	E_4
$\|\frac{1}{2},-1;\frac{1}{2},-1\rangle\otimes\|M_N,M_N'\rangle-\|\frac{1}{2},-1;\frac{1}{2},-1\rangle\otimes\|M_N',M_N\rangle$	15	A_6	E_4
$\|\frac{1}{2},1;\frac{1}{2},-1\rangle\otimes\|M_N,M_N'\rangle+\|\frac{1}{2},1;\frac{1}{2},-1\rangle\otimes\|M_N',M_N\rangle$ $\|\frac{1}{2},-1;\frac{1}{2},1\rangle\otimes\|M_N',M_N\rangle+\|\frac{1}{2},-1;\frac{1}{2},1\rangle\otimes\|M_N,M_N'\rangle$	21	E_1	E_1
$\|\frac{1}{2},1;\frac{1}{2},-1\rangle\otimes\|M_N,M_N'\rangle-\|\frac{1}{2},1;\frac{1}{2},-1\rangle\otimes M_N',M_N\rangle$ $\|\frac{1}{2},-1;\frac{1}{2},1\rangle\otimes\|M_N',M_N\rangle-\|\frac{1}{2},-1;\frac{1}{2},1\rangle\otimes\|M_N,M_N'\rangle$	15	E_1	E_2
$\|\frac{3}{2},0;\frac{1}{2},1\rangle\otimes\|M_N,M_N'\rangle$ $\|\frac{1}{2},1;\frac{3}{2},0\rangle\otimes\|M_N',M_N\rangle$	72	E_2	G
$\|\frac{1}{2},-1;\frac{3}{2},0\rangle\otimes\|M_N',M_N\rangle$ $\|\frac{3}{2},0;\frac{1}{2},-1\rangle\otimes\|M_N,M_N'\rangle$	72	E_3	G

TABLE VIII. Multiplication table of P_{18} irreps.

	A_2	A_3	A_4	A_5	A_6	E_1	E_2	E_3
A_2	A_1							
A_3	A_5	A_4						
A_4	A_6	A_1	A_3					
A_5	A_3	A_6	A_2	A_4				
A_6	A_4	A_2	A_5	A_1	A_3			
E_1	E_1	E_3	E_2	E_3	E_2	$A_1\oplus A_2\oplus E_1$		
E_2	E_2	E_1	E_3	E_1	E_3	$A_4\oplus A_6\oplus E_2$	$A_3\oplus A_5\oplus E_3$	
E_3	E_3	E_2	E_1	E_2	E_1	$A_3\oplus A_5\oplus E_3$	$A_1\oplus A_2\oplus E_1$	$A_4\oplus A_6\oplus E_2$

Downloaded 13 Jun 2006 to 128.32.220.140. Redistribution subject to AIP license or copyright, see http://jcp.aip.org/jcp/copyright.jsp

ries thus obtained for $\nu \equiv A_2$ can be written succinctly in a form known from the representation theory of the permutation group,

$$\Phi^{\lambda}=\frac{1}{\sqrt{f_\lambda}} \sum_{p=1}^{f_\lambda} (-1)^{p+1} \psi_p^{\lambda} \theta_{\tilde{p}}^{\tilde{\lambda}}, \tag{A6}$$

where the ψ_p^{λ} are the spatial basis functions of Table VI and the $\theta_{\tilde{p}}^{\tilde{\lambda}}$ are the spin functions of Table VII. The irrep $\tilde{\lambda}$ is associate to λ. From Table VIII we find that associate pairs are (A_1,A_2), (A_3,A_6), (A_4,A_5), (E_1,E_1) and (E_2,E_3) The index $\tilde{p}$ counts backwards, i.e., $\tilde{p}=f_\lambda+1-p$. The overall phase of the CG series Eq. (A6) is not determined by Eq. (A5) and can be chosen arbitrarily. From Eq. (A6) it follows that each irrep λ of P_{18} corresponds exactly to one antisymmetric ket of definite nitrogen and proton spin magnetic quantum numbers. The number of spin functions N given in Table VII agrees with the spin statistical weights of Nelson and Klemperer.[8] Note that Eq. (A6) in fact defines $(2J+1)\times N$ kets, differing in their nuclear and rotational space-fixed magnetic quantum numbers.

In order to study the first-order quadrupole interaction with the ^{14}N nuclei, we write the usual Hamiltonian as an inner product of two second-rank tensor operators

$$H_Q=\sum_X \mathbf{q}^X \cdot \mathbf{Q}^X \equiv \mathbf{q}^A \cdot \mathbf{Q}^A + \mathbf{q}^B \cdot \mathbf{Q}^B, \tag{A7}$$

where $\mathbf{q}^X$ is the field gradient operator and $\mathbf{Q}^X$ the nuclear quadrupole operator, $X=A$ or B. Substitution of Eq. (A6) gives the following matrix element between two antisymmetric basis functions:

$$\langle \Phi^{\lambda} | H_Q | \overline{\Phi}^{\lambda} \rangle = \frac{1}{f_\lambda} \sum_X \sum_{p,q} (-1)^{p+q} \langle \psi_p^{\lambda} | \mathbf{q}^X | \overline{\psi}_q^{\lambda} \rangle \cdot \langle \theta_{\tilde{p}}^{\tilde{\lambda}} | \mathbf{Q}^X | \theta_{\tilde{q}}^{\tilde{\lambda}} \rangle. \tag{A8}$$

In Table II the effect of $\hat{I}_1$ and $\hat{I}_2$ on the basis is given. We see that for $k_A \not\equiv k_B \pmod 3$ the kets $|k_A,k_B\rangle$ and $\hat{I}_1|k_A,k_B\rangle$ belong to different irreps of $C_3^A \otimes C_3^B$ and hence are orthogonal. If $k_A \not\equiv -k_B \pmod 3$ the same is true for $|k_A,k_B\rangle$ and $\hat{I}_2|k_A,k_B\rangle$. Since $\mathbf{q}^A$ and $\mathbf{q}^B$ commute with $C_3^A \otimes C_3^B$, we find upon consultation of Table VI for the operator matrix elements,

$$\langle \psi_p^{\lambda} | \mathbf{q}^X | \overline{\psi}_q^{\lambda} \rangle = \delta_{pq} \langle \psi_p^{\lambda} | \mathbf{q}^X | \overline{\psi}_p^{\lambda} \rangle. \tag{A9}$$

Many of these elements, diagonal in p, are equal. Using

$$\mathbf{q}^B = \hat{I}_1 \mathbf{q}^A \hat{I}_1 = \hat{I}_2 \mathbf{q}^A \hat{I}_2, \tag{A10}$$

$$\hat{I}_2 |\psi_1^{E_1}\rangle \equiv \hat{I}_2 (\hat{E}+\hat{I}_2) |1,-1\rangle = |\psi_1^{E_1}\rangle, \tag{A11}$$

we find, for instance,

$$\begin{aligned} \langle \psi_2^{E_1} | \mathbf{q}^A | \overline{\psi}_2^{E_1} \rangle &\equiv \langle \psi_1^{E_1} | \hat{I}_1 \mathbf{q}^A \hat{I}_1 | \overline{\psi}_1^{E_1} \rangle \\ &= \langle \psi_1^{E_1} | \mathbf{q}^B | \overline{\psi}_1^{E_1} \rangle \\ &= \langle \psi_1^{E_1} | \hat{I}_2 \mathbf{q}^B \hat{I}_2 | \overline{\psi}_1^{E_1} \rangle \\ &= \langle \psi_1^{E_1} | \mathbf{q}^A | \overline{\psi}_1^{E_1} \rangle. \end{aligned} \tag{12}$$

TABLE IX. Multiplication table of G_{36} irreps.

	A_2	A_3	A_4	E_1	E_2	E_3	E_4	G
A_2	A_1							
A_3	A_4	A_1						
A_4	A_3	A_2	A_1					
E_1	E_1	E_2	E_2	$A_1 \oplus A_2 \oplus E_1$				
E_2	E_2	E_1	E_1	$A_3 \oplus A_4 \oplus E_2$	$A_1 \oplus A_2 \oplus E_1$			
E_3	E_4	E_3	E_4	G	G	$A_1 \oplus A_3 \oplus E_3$		
E_4	E_3	E_4	E_3	G	G	$A_2 \oplus A_4 \oplus E_4$	$A_1 \oplus A_3 \oplus E_3$	
G	G	G	G	$E_3 \oplus E_4 \oplus G$	$E_3 \oplus E_4 \oplus G$	$E_1 \oplus E_2 \oplus G$	$E_1 \oplus E_2 \oplus G$	$G \oplus \Sigma_{i=1}^{4}(A_i \oplus E_i)$

Similarly, we can find equalities across different irreps of P_{18}, e.g.

$$\begin{aligned} \langle \psi^{A_3} | \mathbf{q}^A | \overline{\psi}^{A_3} \rangle &= \langle \psi^{A_4} | \mathbf{q}^A | \overline{\psi}^{A_4} \rangle \\ &= \langle \psi^{A_3} | \mathbf{q}^B | \overline{\psi}^{A_3} \rangle \\ &= \langle \psi^{A_4} | \mathbf{q}^B | \overline{\psi}^{A_4} \rangle. \end{aligned}$$

A quadrupole coupling constant being the expectation value of $\mathbf{q}^X$ with respect to a van der Waals state, it follows that for every irrep of G_{36} there is just one such coupling constant, except for the G representation, where the matrix elements $\langle \psi_1^G | \mathbf{q}^A | \overline{\psi}_1^G \rangle$ *cannot* be shown to be equal to $\langle \psi_1^G | \mathbf{q}^B | \overline{\psi}_1^G \rangle$ by the procedure just outlined.

In order to simplify Eq. (A8), we may apply the same procedure to the spin matrix elements, since the nitrogen quadrupole operators $\mathbf{Q}^X$ satisfy the equivalent of Eq. (A10) and the spin kets of Table VII satisfy the equivalent of Eq. (A11). The unique first-order quadrupole splitting matrix elements that remain to be evaluated are (with the irrep label λ now referring to G_{36}, and the functions ψ_1^{λ}, $\theta_1^{\tilde{\lambda}}$, and $\theta_2^{\tilde{\lambda}}$ being defined in Tables VI and VII, respectively)

$$\langle \Phi^{\lambda} | H_Q | \overline{\Phi}^{\lambda} \rangle = 2 \langle \psi_1^{\lambda} | \mathbf{q}^A | \overline{\psi}_1^{\lambda} \rangle \cdot \langle \theta_1^{\tilde{\lambda}} | \mathbf{Q}^A | \theta_1^{\tilde{\lambda}} \rangle \quad \text{for all } \lambda \neq G \tag{A13}$$

and

$$\langle \Phi^G | H_Q | \overline{\Phi}^G \rangle = \langle \psi_1^G | \mathbf{q}^A | \overline{\psi}_1^G \rangle \cdot \langle \theta_2^G | \mathbf{Q}^A | \theta_2^G \rangle + \langle \psi_1^G | \mathbf{q}^B | \overline{\psi}_1^G \rangle \cdot \langle \theta_2^G | \mathbf{Q}^B | \theta_2^G \rangle. \tag{A14}$$

From Table IX we find the pairs of G_{36} irreps, denoted by Γ and Γ^{spin} in the main text, that can give Pauli allowed functions, i.e., space-spin functions containing an A_2 or an A_4 component. Recall in this connection that A_2 and A_4 only differ under space inversion.

This is as far as G_{36} can simplify the calculation of the quadrupole splittings. In principle, we must now solve $(2J+1)\times N$-dimensional secular problems of H_Q with matrix elements (A13) or (A14). In order to proceed, we may consider the angular momenta involved, i.e., turn to the groups SO(3) and SU(2), which—since they commute with G_{36}—may be considered independently from G_{36}. It is well known for free NH_3 that the operator $\hat{F}^2$, defined by $\hat{\mathbf{F}} \equiv \hat{\mathbf{J}} + \hat{\mathbf{I}}_N$, commutes with H_Q. Vector coupling of the spa-

Downloaded 13 Jun 2006 to 128.32.220.140. Redistribution subject to AIP license or copyright, see http://jcp.aip.org/jcp/copyright.jsp

tial eigenkets of $\hat{J}^2$ with the ^{14}N spin kets then blocks out the first-order secular problem of H_Q. In the present case of two nitrogen spins, one can couple the two momenta with $\hat{\mathbf{J}}$ to $\hat{F}^2$, defined by $\hat{\mathbf{F}} \equiv \hat{\mathbf{J}} + \hat{\mathbf{I}}_{N_A} + \hat{\mathbf{I}}_{N_B}$ which commutes with $\Sigma_X \mathbf{q}^X \cdot \mathbf{Q}^X$. We will not work out in detail the spin matrix elements, suffice it to mention that the proton spin functions integrate out and lead only to Kronecker deltas. The splitted energies are obtained from the solution of small secular problems. The magnitudes of the splittings are solely determined by the quadrupole coupling constants and the value of the ^{14}N quadrupoles.

In the case of G symmetry and $\Omega=0$, the computation of the quadrupole coupling constants requires the evaluation of the matrix elements over the spatial basis of Eq. (6),

$$\langle \psi_1^G | \mathbf{q}^X | \overline{\psi}_1^G \rangle \equiv \langle j_A 0 j_B 1 j 0 J M n | \mathbf{q}^X | j'_A 0 j'_B 1 j' 0 J M' n' \rangle. \tag{A15}$$

Assuming that the field gradient on monomer X ($=A$ or B) is not affected by the other monomer, we may write the components of the operator $\mathbf{q}^X$ as[22]

$$q_m^X = q_0 \sum_\nu D_{m\nu}^{(2)*}(\alpha,\beta,0) D_{\nu 0}^{(2)*}(\gamma_X,\vartheta_X,\varphi_X), \quad m=-2,\ldots,2, \tag{A16}$$

where the component q_0 is the only nonvanishing component of $\mathbf{q}^X$ expressed in the principal axes frame of the free monomer X. From the internal part

$$\langle j_A k_A j_B k_B j \Omega n | D_{\nu 0}^{(2)*} | j'_A k'_A j'_B k'_B j' \Omega n' \rangle. \tag{A17}$$

of the matrix elements (A15) it follows that, for $\Omega=0$, only the term with $\nu=0$ contributes. Recalling that

$$D_{00}^{(2)*}(\gamma_X,\vartheta_X,\varphi_X) = P_2(\cos\vartheta_X), \tag{A18}$$

Eq. (A15) becomes

$$\langle \psi_1^G | \mathbf{q}^X | \overline{\psi}_1^G \rangle \propto \langle j_A 0 j_B 1 j 0 n | P_2(\cos\vartheta_X) | j'_A 0 j'_B 1 j' 0 n' \rangle, \tag{A19}$$

with the proportionality factor being given by q_0 times the integral over α and β. Upon substitution of the CG series of Eq. (6), integration over the internal coordinates γ_B, ϑ_B, φ_B and the distance R, and use of the Wigner–Eckart theorem for $\mathbf{q}^A$, Eq. (A19) becomes for $X=A$,

$$\langle \psi_1^G | \mathbf{q}^A | \overline{\psi}_1^G \rangle \propto \delta_{j_B j'_B} \delta_{nn'} \langle j_A 0 | | P_2(\cos\vartheta_A) | | j'_A 0 \rangle \zeta_{j_A j'_A j_B}, \tag{A20}$$

where $\zeta_{j_A j'_A j_B}$ is a simple algebraic factor consisting of a sum of products of three CG coefficients. The reduced matrix element is the field gradient sandwiched between two *ortho* ($k_A=0$) basis functions of free NH_3. This matrix element appears in the coupling constant $\langle P_2(\cos\vartheta_o)\rangle$, discussed in the main text.

If we next substitute $X=B$ into (A19), we obtain along the very same lines

$$\langle \psi_1^G | \mathbf{q}^B | \overline{\psi}_1^G \rangle \propto \delta_{j_A j'_A} \delta_{nn'} \langle j_B 1 \| P_2(\cos\vartheta_B) \| j'_B 1 \rangle \zeta_{j_A j_B j'_B}. \tag{A21}$$

These reduced matrix elements appear only in the *para* ($k_B=1$) expectation value $\langle P_2(\cos\vartheta_p)\rangle$. Since the first order quadrupole splittings of states of G symmetry contain $\langle P_2(\cos\vartheta_o)\rangle$ and $\langle P_2(\cos\vartheta_p)\rangle$ weighted by different nuclear spin factors, cf. Eq. (A14), measurement of the splittings allows the separate determination of these expectation values.[2]

Next, we turn to the dipole operator $\boldsymbol{\mu}=\boldsymbol{\mu}^A+\boldsymbol{\mu}^B$. Under the assumptions discussed in the main text, the components of this operator can be written in a form similar to Eq. (A16),

$$\mu_m^X = \mu_0 \sum_v d_v(R) D_{mv}^{(1)*}(\alpha,\beta,0) D_{v0}^{(1)*}(\gamma_X,\vartheta_X,\varphi_X), \quad m=-1,0,1, \tag{A22}$$

where μ_0 is the dipole moment of the free NH_3. An explicit expression for $d_v(R)$ is given in Ref. 6. The dipole operator satisfies relations equivalent to (A10),

$$\boldsymbol{\mu}^B = \hat{I}_1 \boldsymbol{\mu}^A \hat{I}_1 = -\hat{I}_2 \boldsymbol{\mu}^A \hat{I}_2. \tag{A23}$$

Furthermore, $\boldsymbol{\mu}$ is invariant under $\hat{R}_1$ and $\hat{R}_2$, so that it transforms as A_3 of G_{36} and as A_1 of P_{18}.

Since $\boldsymbol{\mu}$ does not act on nuclear spin, we can integrate out the spin coordinates. From the analogue of (A8) and (A9) (with irrep labels referring to P_{18}),

$$\langle \Phi^\lambda | \boldsymbol{\mu} | \overline{\Phi}^\lambda \rangle = \frac{1}{f_\lambda} \sum_p \langle \psi_p^\lambda | \boldsymbol{\mu} | \overline{\psi}_p^\lambda \rangle. \tag{A24}$$

Note that this matrix element is an unweighted average over the partners in a P_{18} irrep, while in the corresponding expression (A8) for the quadrupole coupling the terms are weighted by spin matrix elements.

Using Eq. (A22) and performing the integration over the external angles α and β, we find the result, which is well known for rigid symmetric tops, that dipole matrix elements diagonal in J vanish for $\Omega=0$. The $\Omega=0$ states of the dimer do not exhibit first order splittings when perturbed with $-\boldsymbol{\mu}\cdot\mathbf{E}$, the interaction of the dimer with an external electric field $\mathbf{E}$. For $\Omega\neq 0$ first order Stark splittings may be observed, though, provided the internal motions do not forbid them.

The internal motions that allow a first order Stark splitting are easily found by the procedure of Eq. (A12), with the rules of (A23) instead of (A10). Thus, we can show that for $\lambda=A_1$, A_2, and E_1 the expression (A24) vanishes, whereas for the P_{18} pairs $(\lambda,\lambda^*)=(A_3,A_4)$, (A_5,A_6), (E_2,E_3)—connected by I_2—we find that

$$\sum_p \langle \psi_p^\lambda | \boldsymbol{\mu} | \overline{\psi}_p^\lambda \rangle = -\sum_p \langle \psi_p^{\lambda^*} | \boldsymbol{\mu} | \overline{\psi}_p^{\lambda^*} \rangle. \tag{A25}$$

Because the direct sums $\lambda \oplus \lambda^*$ are irreps of G_{36} (see Table VI), it follows that, upon averaging over partners in an irrep of the latter group, all expectation values of $\boldsymbol{\mu}$ vanish. In a Stark measurement parity is broken, however, and the symmetry of the system is lowered to P_{18}. It follows immediately from (A25) that the degenerate E_3, E_4, and G states split in first order under the influence of an electric field. Using the model dipole (A22) and applying the pro-

Downloaded 13 Jun 2006 to 128.32.220.140. Redistribution subject to AIP license or copyright, see http://jcp.aip.org/jcp/copyright.jsp

cedure developed in Eqs. (A15) through (A21), we can easily show that the Stark splitting of an $|\Omega|>0$ state of G symmetry depends on the sum $\langle P_1(\cos\vartheta_o)\rangle + \langle P_1(\cos\vartheta_p)\rangle$. The Stark splittings of E_3 and E_4 states depend only on $\langle P_1(\cos\vartheta_A)\rangle = \langle P_1(\cos\vartheta_B)\rangle = \langle P_1(\cos\vartheta_p)\rangle$.

Let us finally discuss the selection rules for pure rotational transitions, illustrated in Fig. 6. Without off-diagonal Coriolis interaction the pure rotational ladders

$$|JM\Omega\rangle|\lambda\Omega\rangle \quad \text{and} \quad |JM-\Omega\rangle\hat{I}_1|\lambda\Omega\rangle, \quad J=1,2,... \tag{A26}$$

are pairwise degenerate for $\Omega\neq 0$. The external ket $|JM\Omega\rangle \propto D^{(J)*}_{M\Omega}(\alpha,\beta,0)$ depends only on α and β, and $|\lambda\Omega\rangle$ is a shorthand notation for the part of the van der Waals state depending only on the internal coordinates. Since the external ket is invariant under the generators $\hat{R}_1$, $\hat{R}_2$, and $\hat{I}_2$, the kets in (A26) transform as λ of $C_3^{ag}\otimes C_{3v}^{g}$, a group obtained from G_{36} by removal of $\hat{I}_1$. When we switch on the Coriolis interaction, the energies of the kets

$$|JM\Omega\rangle|\lambda\Omega\rangle \pm |JM-\Omega\rangle\hat{I}_1|\lambda\Omega\rangle \tag{A27}$$

will be slightly split in the following cases, which are listed by indicating their correlation $C_3^{ag}\otimes C_{3v}^{g}\subset G_{36}$, cf. the discussion in the first paragraph of Sec. V,

$$\begin{aligned} &A_1\otimes A_1 \rightarrow A_1,A_2,\\ &A_1\otimes A_2 \rightarrow A_3,A_4,\\ &A_1\otimes E \rightarrow E_3,E_4. \end{aligned} \tag{A28}$$

Noting that $\hat{I}_1|JM\Omega\rangle = (-1)^J|JM-\Omega\rangle$, cf. Table II, we find from

$$\begin{aligned} &\hat{I}_1(|JM\Omega\rangle|\lambda\Omega\rangle \pm |JM-\Omega\rangle\hat{I}_1|\lambda\Omega\rangle)\\ &\quad = \pm(-1)^J(|JM\Omega\rangle|\lambda\Omega\rangle \pm |JM-\Omega\rangle\hat{I}_1|\lambda\Omega\rangle), \end{aligned} \tag{A29}$$

that for even J the plus combination (A27) is symmetric under $\hat{I}_1$ and for odd J it is antisymmetric. If we step through the rotational ladders of Eq. (A28) with $\Delta J=1$, the irreps alternate between A_1/A_2, A_3/A_4, and E_3/E_4, respectively. For the minus combination of Eq. (A27), we find the same result with the roles of even and odd J reversed. We thus have three pairs of rotational ladders with energy separations modified by off-diagonal Coriolis interactions. Only pure rotational transitions from the plus to the minus E_3/E_4 ladder—and vice versa—can be observed, since the G_{36} selection rules forbid those for the other four ladders. Note that this selection rule is consistent with the fact that the internal functions of A symmetry do not have dipoles, whereas those of E_3 and E_4 symmetry have nonvanishing dipoles.

In the remaining three cases Coriolis interaction does not give a splitting, so that the linear combinations (A27) do not have to be taken. These cases are

$$\begin{aligned} &\{A_2\otimes A_1, A_3\otimes A_1\}\rightarrow E_1,\\ &\{A_2\otimes A_2, A_3\otimes A_2\}\rightarrow E_2,\\ &\{A_2\otimes E, A_3\otimes E\}\rightarrow G. \end{aligned} \tag{A30}$$

Only $G\leftrightarrow G$ is an observable $\Delta J=1$ pure rotational transition, the other two ladders of Eq. (A30) do not support allowed $\Delta J=1$ transitions. Note that this selection rule is consistent with the fact that the internal functions of G symmetry give a nonvanishing dipole, as we have discussed above.

[1] A. D. Buckingham, P. W. Fowler, and J. M. Hutson, Chem. Rev. **88**, 963 (1988).
[2] D. D. Nelson, G. T. Fraser, and W. Klemperer, J. Chem. Phys. **83**, 6201 (1985).
[3] D. D. Nelson, W. Klemperer, G. T. Fraser, F. J. Lovas, and R. D. Suenram, J. Chem. Phys. **87**, 6364 (1987).
[4] K. P. Sagarik, R. Ahlrichs, and S. Brode, Mol. Phys. **57**, 1247 (1986).
[5] D. M. Hassett, C. J. Marsden, and B. J. Smith, Chem. Phys. Lett. **183**, 449 (1991).
[6] J. W. I. van Bladel, A. van der Avoird, and P. E. S. Wormer, J. Phys. Chem. **95**, 5414 (1991).
[7] G. T. Fraser, D. D. Nelson, A. C. Charo, and W. Klemperer, J. Chem. Phys. **82**, 2535 (1985).
[8] D. D. Nelson and W. Klemperer, J. Chem. Phys. **87**, 139 (1987).
[9] A. van der Avoird, P. E. S. Wormer, F. Mulder, and R. M. Berns, in *van der Waals Systems*, edited by Michael J. Dewar *et al.*, Vol. 93, in *Topics in Current Chemistry* (Springer-Verlag, Berlin, 1980), p. 1.
[10] G. Brocks, A. van der Avoird, B. T. Sutcliffe, and J. Tennyson, Mol. Phys. **50**, 1025 (1983)
[11] P. R. Bunker, W. P. Kraemer, and V. Špirko, Can. J. Phys. **62**, 1801 (1984).
[12] *Handbook of Chemistry and Physics* (CRC, Cleveland, 1974–1975).
[13] J. Tennyson and B. T. Sutcliffe, J. Chem. Phys. **77**, 4061 (1982); **79**, 43 (1983).
[14] P. R. Bunker, *Molecular Symmetry and Spectroscopy* (Academic, New York, 1979).
[15] C. E. Dykstra and L. Andrews, J. Chem. Phys. **92**, 6043 (1990).
[16] M. D. Marshall and J. S. Muenter, J. Mol. Spectrosc. **85**, 322 (1981).
[17] P. E. S. Wormer and H. Hettema, J. Chem. Phys. (submitted).
[18] E. Zwart, Ph.D. thesis, Nijmegen, 1991 (unpublished).
[19] M. Havenith, R. C. Cohen, K. L. Busarow, D-H. Gwo, Y. T. Lee, and R. J. Saykally, J. Chem. Phys. **94**, 4776 (1991).
[20] J. G. Loeser, C. A. Schmuttenmaer, R. C. Cohen, M. J. Elrod, R. J. Saykally, R. E. Bumgarner, and G. A. Blake, J. Chem. Phys. **97**, 4727 (1992), preceding paper.
[21] M. D. Marshall, P. Jensen, and P. R. Bunker, Chem. Phys. Lett. **176**, 255 (1991).
[22] J. W. I. van Bladel, A. van der Avoird, and P. E. S. Wormer, Chem. Phys. (in press).

Downloaded 13 Jun 2006 to 128.32.220.140. Redistribution subject to AIP license or copyright, see http://jcp.aip.org/jcp/copyright.jsp